Meteorol. Atmos. Phys. 72, 161–173 (2000)

Meteorology and Atmospheric Physics

Deutsches Zentrum für Luft- und Raumfahrt (DLR), Institut für Physik der Atmosphäre, Oberpfaffenhofen, Germany

Precipitation in the Northern Alpine Region: Case-Study-Type Validation of an Operational Forecast Model

C. Keil and **H. Volkert**

With 10 Figures

Received March 2, 1999
Revised July 28, 1999

Summary

Quality and limitations of current quantitative precipitation simulations are determined using the Deutschland-Modell of Deutscher Wetterdienst (DWD). The model independent validation data comprise the regular rain-gauge network of DWD, taylored composites of an international radar network, Doppler winds from the DLR research radar, and meteorological timeseries at a ground station. Area skill scores are compared for convectively dominated as well as more synoptically forced situations in the northern Alpine region. Inspection of the temporal evolution of the components comprising the atmospheric water budget and of the precipitation partition gives insight in the different nature of excitation mechanisms of heavy precipitation. The simulations are found to exhibit growing potential for follow-on hydrological applications, while a real breakthrough appears to necessitate the coming generation of non-hydrostatic operational forecast models with increased spatial resolution.

1. Introduction

The Alpine precipitation climatology exhibits characteristic seasonal variations in the northern Alpine region, where enhanced precipitation is observed during the main convective period from May until September (Frei and Schär, 1998). Distinct seldom occuring events of heavy precipitation, like the development of mesoscale convective systems or rainfall episodes enhanced by orographic blocking, contribute significantly to the annual mean precipitation and are able to trigger natural disasters as, e.g., wide area flooding, flash floods, landslides or serious cases of hail damage. Sufficiently precise forecasts of such severe precipitation events one to three days in advance could significantly contribute to avoid loss of life and reduce damage.

Presently regional numerical weather prediction (NWP) models are operationally applied to gain short-range forecasts with a horizontal spatial resolution approaching 10 km. With the currently available computer resources, such high resolution models are only feasible for a limited domain, i.e. in the regional or meso-scale. Thus the large-scale meteorological evolution has to be passed on through time dependent lateral boundary conditions. The atmospheric processes which control precipitation to a large extent act on the meso-scale (typical lateral extents between 1 and 1000 km) and render a precise rainfall prediction considerably more difficult than, e.g., a pressure, wind or temperature forecast. Many complex atmospheric processes resulting in a highly variable spatio-temporal precipitation distribution can only partly be explicitly incorporated in such meso-scale models. The remaining unresolved processes have to be parameterized and pose the cumulus parameterization problem (see, e.g., the overview article by Molinari and Dudek, 1992). Consequently precipitation shows the greatest

Table 1. *List of Investigated HERA Cases. The Precipitation Amounts (RR_{obs}) Denote the Observed Daily Area Average and the Observed Maxima (RR_{max}) with their Locations (Latitude ϕ_{max}, Longitude λ_{max})*

Date	Synoptic Type	RR_{obs} (mm/d)	RR_{max} (mm/d)	ϕ_{max} (deg.)	λ_{max} (deg.)
5 July 1996	cold front with intense prefrontal squall	14.3	89.0	48.2	7.9
8 July 1996	cyclogenesis over the Alps	24.2	124.9	47.7	12.3
4 July 1994	Mesoscale Convective System	10.8	96.5	47.8	10.1
14 July 1994	Mesoscale Convective System	6.4	57.9	49.1	8.2

sensitivity to the model physics and its prediction continues to be one of the great challenges in atmospheric modelling.

A detailed assessment of an atmospheric model's capabilities constitutes one important quality control step. The validation of the precipitation distribution, in particular, represents a substantial task because of its aforementioned intrinsic spatial and temporal variability. Moreover evaluation difficulties emerge from the severe gap between the spatial density of traditionally used rain gauge observations and the calculated data. Radar data, on the other hand, offer precipitation estimates with high spatial resolution and have not yet been widely used for NWP model validation. Up to very recently the routine verification of precipitation by the national weather services was restricted to seasonal rainfall means validated with precipitation observations at selected synoptic stations. Such a method veils information about the model's accuracy for individual episodes of severe precipitation. The latest, more precise evaluations undertaken by European meteorological services are not available in the open literature. Therefore it is felt that our assessment regarding a few episodes possesses significant explorative character.

Reliable forecasts of the mesoscale precipitation patterns are seen as an essential prerequisite for physically based hydrological forecasting schemes including (flash) flood warning procedures with a lead time of two or more days, particularly in mountainous terrain. Within the project HERA regional simulations of four northern Alpine episodes with considerable rainfall amounts were performed with the operational forecast model of DWD (Table 1). One of them is discussed here in detail to highlight the potential of quantitative precipitation forecasts as well as its actual limitations.

After a short description of the forecast model an overview of the synoptic scale weather situations is presented. Subsequently the simulation results are compared with various background observations comprising high resolution rain gauge measurements, taylored composites of a precipitation radar network and timeseries of meteorological parameters recorded at a ground station. The radar reflectivities are augmented by Doppler wind velocities to provide a spatial high resolution data set for an evaluation of the simulated flow field. The results of this convective case are juxtaposed to other northern Alpine precipitation episodes whose rainfall patterns were induced by prominent weather situations. Finally the model is used as a diagnostic tool to investigate the atmospheric water budget in a pre-Alpine river catchment. The main findings and a brief outlook are summarized in the concluding section.

2. Model Description and Initial Conditions

The numerical simulations are performed with the hydrostatic Deutschland-Modell (DM; Schrodin, 1997). Introduced in 1993, this regional model is the main short range weather forecasting tool applied by DWD till the end of 1999. The model domain covers central Europe (Fig. 1) encompassing 109×109 grid points with a horizontal mesh size of $\Delta x \approx 14$ km. Vertically the model's atmosphere is discretized in 20 layers on a hybrid coordinate system.

Physical processes associated with cumulus convection are divided in resolvable-scale processes and subgrid-scale processes. Grid-scale precipitation includes parameterized cloud microphysics of the Kessler type and allows for interactions between water vapour, cloud water, rain and ice. Subgrid-scale deep convection processes are parameterized by the traditional

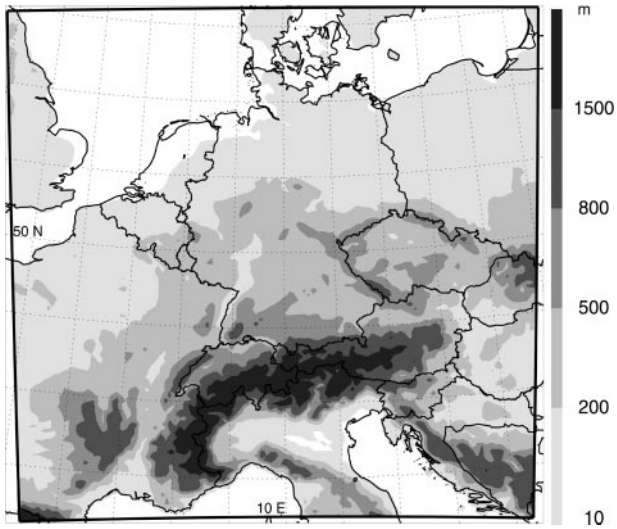

Fig. 1. Domain of DM with coastlines, political boundaries, a $2 \times 2^{\circ}$ geographical grid, and topographic heights of the model orography (grey scale)

Tiedtke mass flux scheme, designed originally for a coarse resolution, where moisture convergence in the sub-cloud layer is the essential mechanism to generate convection (Tiedtke, 1989).

Six-hourly analyses taylored for DM were used as initial and boundary conditions. A Davies type boundary relaxation scheme is applied to adjust the model variables towards the large scale lateral boundary conditions. The model runs were initialized at 00 UT for every individual case. Data of the period $+6$ h till $+30$ h of the simulation are considered, i.e. only values after the model spin-up time.

We note that we cannot determine the entire predictability as if we had used truely forecast boundary conditions, as e.g., in Mladek et al. (this volume). On the other hand, all discrepancies found here have to be attributed to model deficiencies, e.g., insufficient horizontal resolution or too simple physical parameterisations, or to an inappropriate mesoscale analysis scheme.

3. Synoptic Overview

On 5 July 1996 a mesoscale cyclone developed over France embedded in a strong upper tropospheric southwesterly airflow and gradually moved across Germany while still intensifying. Ahead of the cold front warm air was prevailing in southeastern Germany which favoured the formation of deep convection. Along a prefrontal convergence line strong thunderstorm activity was observed.

Subsequently a surface low developed over the Alpine region under the leading edge of an upper level trough extending to the western Mediterranean on 7 July 1996 00 UT. At the border of warm air masses over eastern Central Europe and significantly cooler ones to the west a wide spread precipitation region formed. This area of intense rainfall moved northeastward across the Czech Republic and Poland on 8 July 1996 along the still quoted "route Vb" of last century's catalogue of European storm tracks (Bebber, 1891). Additionally the precipitation got intensified by orographic lifting processes in the northern Alpine region. Under the influx of cool but humid maritime air the temperature in southern Germany only slightly exceeded 10 °C on 8 July 1996.

In contrast to those pronounced meso-α-scale weather situations two mesoscale convective systems (MCS) were observed on 4 July and 14 July 1994 during the Severe Thunderstorm Experiment (SETEX). Emerging from scattered thunderstorms above the Jura and Black Forest mountains rapidly growing MCSs evolved during prefrontal conditions and moved eastward towards Bavaria. Their precipitation signatures had more local character resulting in lower rainfall areal averages (Table 1).

4. Observations and Simulations for 5 July 1996

The simulation quality of DM for a distinct precipitation event is now exemplified in detail for the rainfall episode on 5 July 96. The presentation of observational data follows a decrease in space and time scale and comprises daily precipitation totals in southern Germany, the overall temporal development and motion of the precipitating system as seen by an international radar composite, Doppler-derived radial winds viewed from a single radar station, and local timeseries.

4.1 Daily Precipitation Totals

Traditionally rain gauge observations are used to evaluate the temporally integrated rainfall over

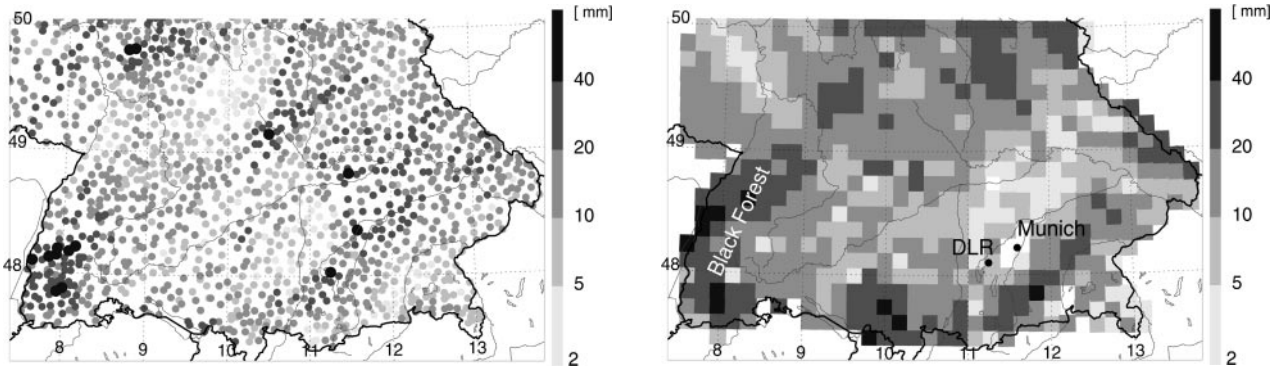

Fig. 2. Observed (left) versus simulated (right) 24 h precipitation totals for 5 July 1996

24 hours. We first note the different nature of the data types. Each model value at a horizontal resolution of 14 km represents an average over an area of about 200 km^2, whereas the actual precipitation can vary significantly over such an area, especially above complex terrain and during convectively dominated conditions. On the other hand the discrete character of rain gauge observations limits their representativity which is influenced by, e.g., the highly variable character of convective precipitation as well as limitations due to the exact location of the gauge within the topography. Nonetheless rain gauge observations are widely used for a quantitative precipitation evaluation.

In Fig. 2 the precipitation distribution on 5 July 1996 is depicted. First of all the spatially heterogeneous character of the convective event becomes evident. The strongest precipitation was observed in the Black Forest mountains in southwestern Germany with a total rainfall of 89 mm. The maximal simulated precipitation yields 56 mm just two mesh widths further west. Another zone with considerable precipitation lies northeastward of Munich where deep convection along the convergence line resulted in rainfall totals of more than 30 mm. In the model prediction a comparable region of enhanced precipitation appears 50 km further to the east with maxima amounting to about 20 mm.

Averaging the irregularly spaced 1031 available rain gauge observations onto the model grid allows a more quantitative comparison. Generally the model slightly overestimates the areal rainfall by 9.6% in southern Germany on 5 July 1996 (see Table 2). Statistical measures of precipitation forecast accuracy are provided in the next section.

4.2 Temporal Overall Development

Now, we examine the spatial and temporal structure of the precipitation fields. Observations of the weather radar networks of the Alpine countries, which are assembled to the HERA North Alpine Radar Composite (Hagen et al., this volume), are qualitatively compared with simulated pseudo-radar images. Once again it is necessary to keep the different nature of the two data types in mind.

Radar detectability of hydrometeors can be seriously affected by their distances from the radar site and by orography intersecting the radar pulses. The main error sources of radar derived rain rates are due to beam blocking, beam broadening and the decrease of reflectivity with height (Joss et al., 1995). In the HERA North Alpine Radar Composite the *radar precipitation estimates* are assigned the maximum precipitation intensity found in a given vertical column, no matter whether it was detected by one or several radars of the network. Thus it is not possible to determine the height of the observed hydrometeors. The precipitation estimates are grouped into six logarithmically scaled intensity levels on a 2 km horizontal grid.

The DM *pseudo-radar images* display maximum precipitation fluxes sampled from the vertical columns of the model grid. The depicted instantaneous precipitation flux results from precipitation forming processes within one model time step. The model precipitation rates

Table 2. *DM-Simulated Precipitation of four HERA Cases comprising Area Averages RR_{DM}, Relative Contribution of Convective Rainfall RR_{conv}, Ratio of Modelled Versus observed Precipitation RR_{DM}/RR_{obs} and the modelled Maxima with their Locations (Latitude ϕ_{max}, Longitude λ_{max})*

Date	RR_{DM} (mm/d)	RR_{conv} (%)	RR_{DM}/RR_{obs} (%)	RR_{max} (mm/d)	ϕ_{max} (deg.)	λ_{max} (deg.)
5 July 1996	15.63	91	109.6	55.5	48.4	7.8
8 July 1996	19.94	24	82.2	123.5	47.5	10.0
4 July 1994	7.49	94	69.0	76.6	47.8	10.2
14 July 1994	12.55	85	196.2	133.3	48.7	11.1

are discretized according to the radar intensity classes for this investigation. In contrast to the higher spatial resolution of the radar data the simulated precipitation flux is only available on the model grid with a "pixel size" of $14 \times 14\,\mathrm{km}^2$.

In Fig. 3 the radar observed convective activity is compared with its simulated counterpart described above. The radars detected a pronounced frontal line with imbedded convection cores, which moved eastward across southern Germany. The leading edge of the convective line approached Munich at 17 UT with high reflectivity values of 55 dBZ indicating heavy precipitation or even hail.

A similiar though patchier structure of an eastward progressing frontal line with high precipitation rates is reproduced by the model. The simulated precipitating region lags the observation by about one hour and crosses the Lake of Constance area at 17 UT. Precipitating processes along that convergence line yield rainrates of up to 31 mm/h. The upward motion, one requirement for the precipitation formation, reaches values up to 1.1 m/s along that frontal line. Relatively warm and humid air ahead of the front sustains the formation of convection. Mesoscale ascent of the humid air yields precipitation rates of 16 mm/h at 19 UT when the convergence line has already crossed Munich. The heights, in which the precipitation flux attains its maximum, vary during this period between 770 hPa and 885 hPa. Below that layer subcloud evaporation reduces the quantity of condensate reaching the earth's surface. With the frontal passage the wind is veering towards west and cooler and drier air gets advected.

The qualitative comparison of radar composites and numerically simulated pseudo-radar images reveals the model's ability to capture the general structure and progression of the convergence line.

Aligned mesoscale convective areas with upward motion are simulated; these are favourable for the initiation and maintainance of convection. Moreover the instantaneous precipitation flux illustrates that Tiedtke's convective parameterization scheme applied in the mesoscale produces a rather patchy precipitation structure. These rainrates result from the convergence of moisture within one single model time step. Since the convective cloud water content is a diagnostic variable, no life cycle of convective clouds is included and, thus, the snapshots of the depicted precipitation flux show an incoherent structure. Integrating the instantaneous rainrates over time yields, e.g., hourly rainfall accumulations with smoother structures (cf. Volkert, this volume; Fig. 7). But at a gridsize of 14 km a snapshot of the precipitation flux at a specific time step of the model integration cannot be expected to show as many details of the convective activity as detected by the radars.

4.3 Doppler Winds

Data taken by DLR's Dopplerized polarization diversity radar (POLDIRAD) are used to retrieve the radial wind field relative to the radar location in Oberpfaffenhofen. Doppler wind measurements are possible when precipitation particles are present in the air volume under examination. Therefore no velocity data are available in the 'dry' (grey coloured) region ahead of the front (Fig. 4). Peak radial velocities were detected in a zone 20 to 50 km WSW (255°) of the radar site, where the Nyquist-corrected signal amounted to 24 m/s in an altitude of about 400 m above ground. The region in which the flow is

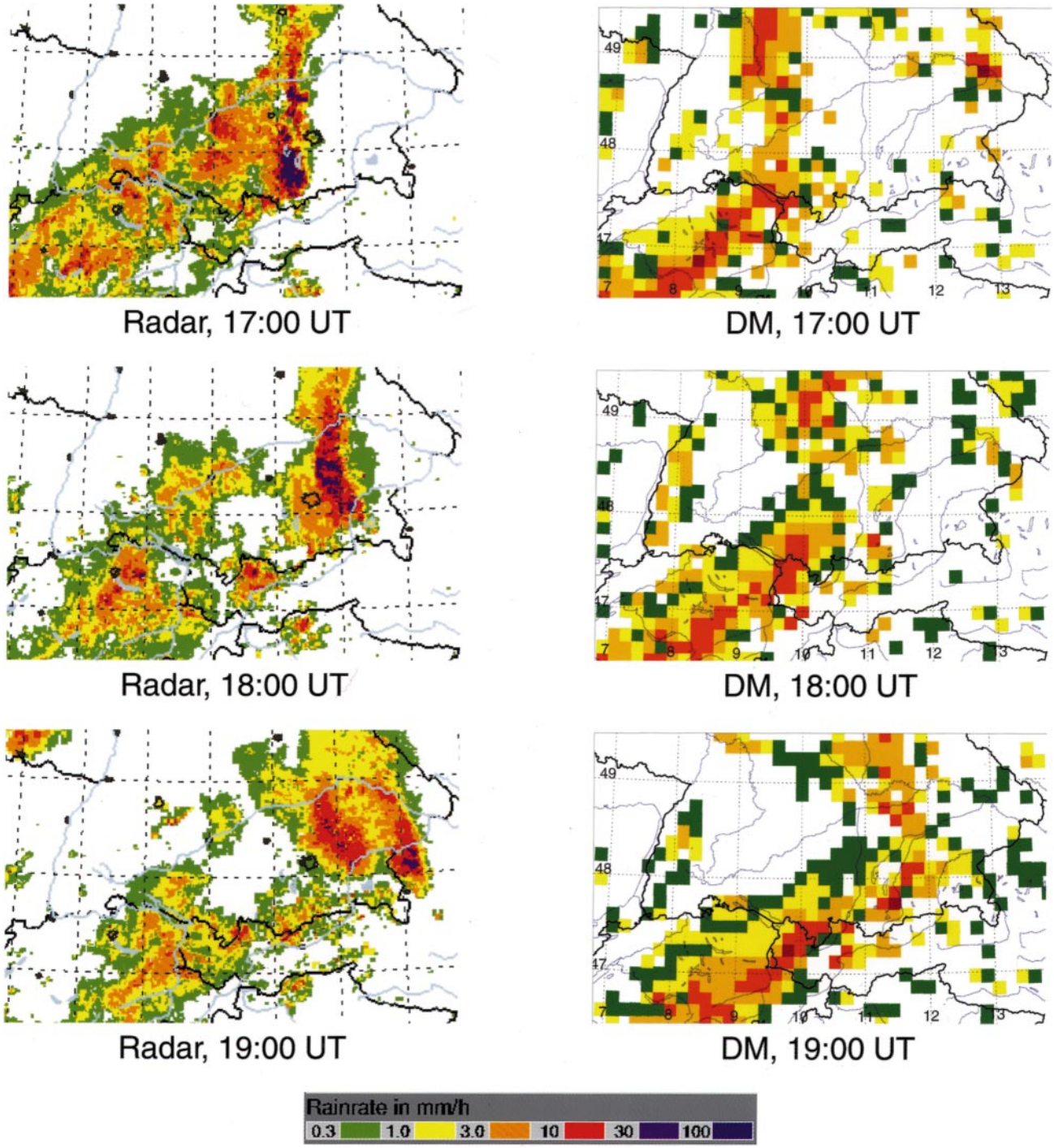

Fig. 3. *Radar composites* of the Swiss, Austrian and German Radar network on 5 July 1996 (left) and instantaneous *pseudo radar images* of the Deutschland Modell simulation (right; colour coded as the radar composites)

perpendicular with respect to the radar site, i.e. the radial velocity diminishes, extends NNW with an angle of 330°. The southern branch of that zone is masked due to the absence of hydrometeors. Ahead of the convergence line weak northerly winds of 2 m/s prevailed south of the radar.

In Fig. 5 the radial component of the simulated horizontal wind field relative to the radar site is shown for a layer 480 m above ground. Main radar detected features of the flow field can be identified in the model data. The maximum of the simulated radial wind velocity is situated WSW (240°) of the radar site, where the southwesterly

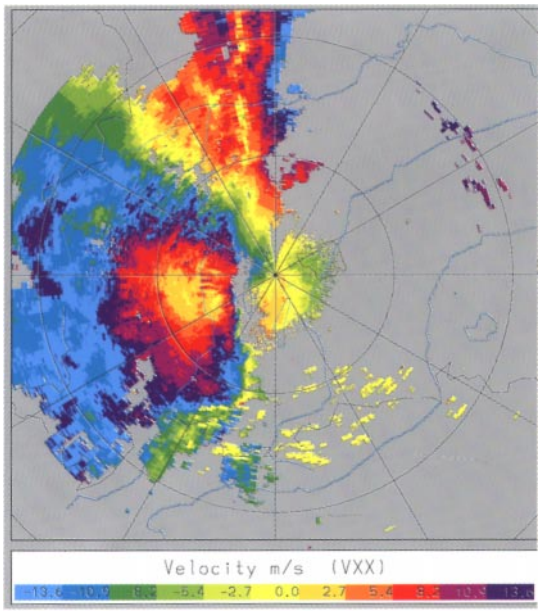

Fig. 4. Doppler radial wind velocity measured by POLDIRAD at Oberpfaffenhofen on 5 July 1996, 16:49 UT with 1° elevation. Negative values indicate a flow directed towards the radar. For technical reasons values below the Nyquist-threshold (− 13.6 m/s) are wrapped to the other side of the colour scale (as due W of the radar site)

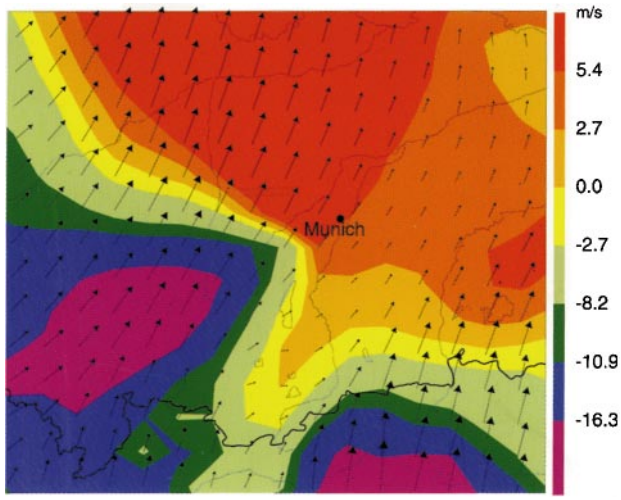

Fig. 5. Simulated radial wind velocity relative to the gridpoint Oberpfaffenhofen (colour coded as the Doppler radial wind in Fig. 4) for 5 July 1996, 18:00 UT and 480 m above ground. The arrows indicate the Cartesian flow components (max. vector equals 25 m/s). A time-lag of 1 h between observations and simulation is taken into account (see subsection 4.4)

flow is directed straight towards the virtual observing station and peaks in 21 m/s. The zone with zero radial velocity values extends from NWN (295°) to SSW (190°) with respect to the virtual radar site. A slight northerly component of the wind vector is predicted for an area about 30 km south of Munich and compares well with the measurements. The secondary maximum at the southern boundary of the depicted region is caused by the Alpine orography, where the wind velocity 480 m above ground exceeds 16.3 m/s.

To the authors' knowledge comparisons between radar Doppler winds and meso-scale flow simulations were sofar not documented for Central Europe. The reasonable agreement between Figs. 4 and 5 is felt as an encouraging one as reliable motion fields are a prerequisite for good precipitation forecasts.

4.4 Local Timeseries

Timeseries of meteorological parameters offer another model independent data source to validate the simulation and to quantify possible timing or phase errors which are frequently contained in the initial data of the simulation.

The weather station at DLR is located atop the building about 15 m above ground. Its timeseries clearly mark the frontal passage (Fig. 6). At 1700 UT the pressure reached its minimum followed by a sharp increase of 4 hPa within 15 min. The temperature concurrently dropped by 8 K down to 16 °C. The gust front crossed the observation platform with wind velocities up to 16 m/s nine minutes later (1709 UT) followed by a narrow zone of heavy precipitation which resulted in 11 mm within 6 min.

Comparing the observed timeseries (data every 3 min.) with the simulated ones (data every 12 min.) at the closest gridpoint the much smoother character of the simulation becomes obvious. The initial and final values of temperature, pressure and wind speed of the depicted 12 hourly timeseries agree remarkably well. A closer look reveals a time difference of one hour between observation and simulation. At 18 UT all of the displayed meteorological parameters indicate the passage of the frontal line. Simultaneously with the steady temperature drop, the pressure and the wind speed increase. The accumulated precipitation caused by the

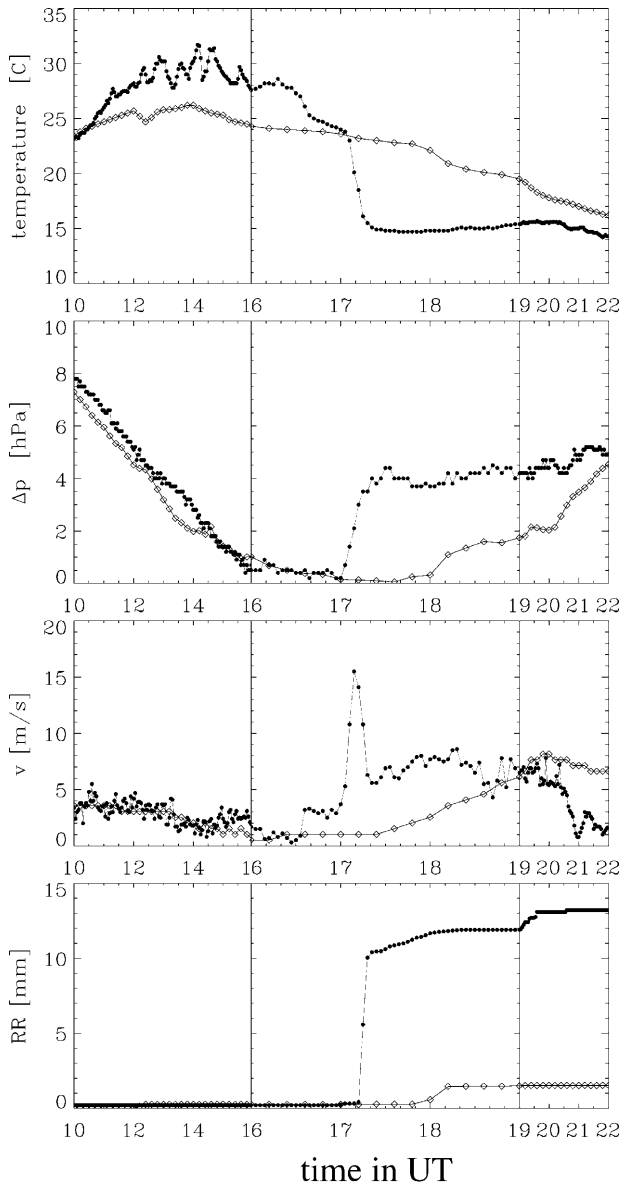

Fig. 6. Observed (bullets) and simulated (diamonds) time-series of temperature, pressure difference (relative to an arbitrary offset), wind speed and precipitation (from top to bottom) in Oberpfaffenhofen on 5 July 1996. In the time interval 16 to 19 UT the abscissa is stretched

convergence line amounts to less than 2 mm in the model.

Clearly the local scale structure and strength of the frontal discontinuity cannot be completely simulated at a grid size of 14 km. But again the coincidence between locally observed and grid-point time-series is considered as an important hint for the feasibility of reliable meso-scale modelling of severe weather events.

5. Results for other HERA Cases

After the close-up looks at details of the weather evolution of 5 July 1996, we now apply statistical measures of precipitation totals to investigate the model's capabilities more generally and present results of other HERA rainfall episodes.

First the precipitation totals of 8 July 1996 are presented in Fig. 7. The uniformity of the values is in some contrast to the much more spatially structured convective pattern three days earlier. The observed, quasi-uniform precipitation distribution had maxima at the northern Alpine rim which amounted to 124.9 mm in 24 hours (see Table 1). The predicted maxima of 123.5 mm compares well in amplitude, although it is displaced by 150 km to the west in the northern Alpine foreland (see Table 2). Orographic lifting processes triggered by the Alps in the southward flow cause these extreme rainfall totals.

The predicted distribution of rainfall totals less than 20 mm along the Upper Danube valley and precipitation accumulations of more than 40 mm only several kilometers northwestward in the Swabian Jura are confirmed by rain-gauge observations. Between 49° and 50° latitude the river Rhine bounds the rainfall region to the west and agrees well with available observational data. Only in eastern Bavaria, in an area between rivers Danube and Inn, the model predicts less than the observed precipitation totals. Hence the DM underpredicts the area averaged rainfall in southern Germany by 18%.

Unfortunately there is no single measure of forecast skill that completely characterizes the accuracy of a precipitation prediction. To quantify the accuracy of the precipitation totals we use the *bias score* and the *threat score* of a specified precipitation threshold amount at a given grid point during a specified time period (Anthes, 1983). The *bias score* measures the tendency of a model to forecast too small or too large an area of a given amount of precipitation, while the *threat score* describes the skill in simulating the exact area of precipitation totals above a given threshold. These areas agree completely if the scores amount to one. A bias score greater than one indicates an overprediction of precipitation.

The calculated scores in Fig. 8 illustrate the case-to-case variability. Generally the bias is

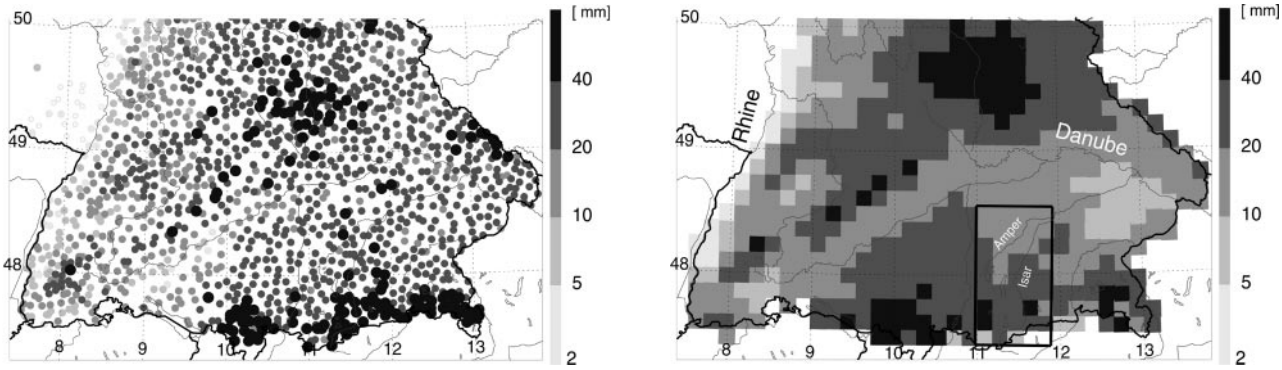

Fig. 7. Observed (left) versus simulated (right) 24 h precipitation totals for 8 July 1996. The *Isar-Amper* catchment as referred to in Figs. 9 and 10 is surrounded by the bold rectangle

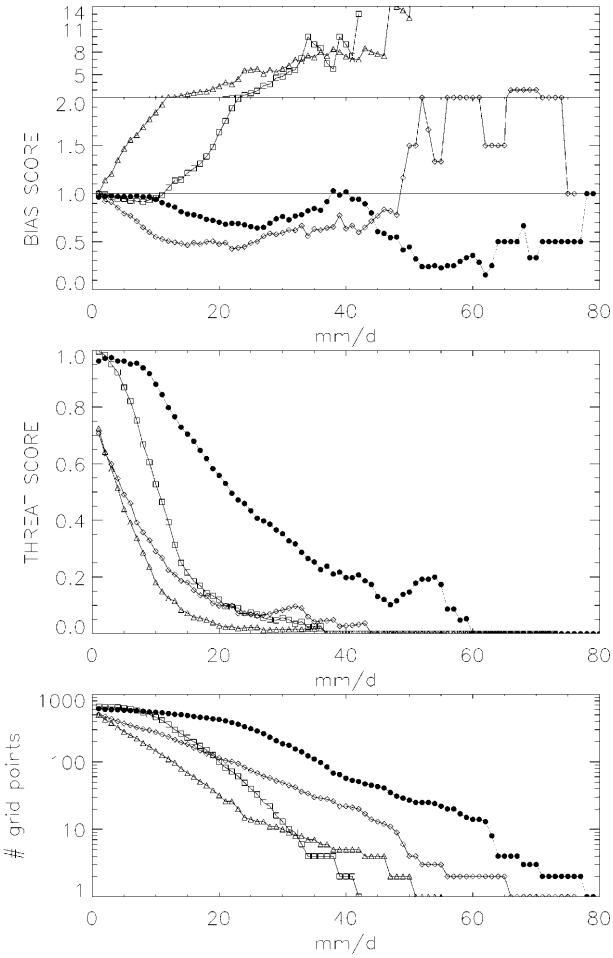

Fig. 8. Rainfall scores for 4 HERA cases versus a prescribed 24 h precipitation threshold. The bias score, threat score and the number of grid cells (top to bottom) are depicted for 5 July 1996 (squares), 8 July 1996 (bullets), 4 July 1994 (diamonds) and 14 July 1994 (triangles). Note the compression of the ordinate for high bias score values (BS $>$ 2). The number of cells receiving more than the threshold amount is based on observations averaged onto the model grid and is scaled logarithmically

increasing for greater precipitation amounts. Bias score values for rainfall thresholds greater than 40 mm may not be meaningful since the number of points receiving this amount is often small (e.g., only 2 grid cells on 5 July 1996, bottom graph in Fig. 8). The bias score shows an overestimation of the precipitation totals exceeding 20 mm for 5 July 96 whereas a slight underrating can be identified for low rainfall thresholds. For the stratiform rainfall event of 8 July 1996 the bias score shows good agreement for precipitation accumulations up to 40 mm. Only scores greater than this threshold reveal the model's underestimation. The threat scores show a decreasing skill with increasing threshold as well. For a threshold of 10 mm the threat scores range from 0.85 to 0.17 for 8 July 1996 and 14 July 1994, respectively. For the 20 mm threshold they range from 0.55 to 0.025. As the area diminishes in size with increasing precipitation threshold correct forecasts become more difficult to obtain. Consequently best scores are determined for the episode on 8 July 1996 with widespread precipitation in southern Germany, when 50 grid points received more than 40 mm. Moreover a quite good threat score is evident for the case of 5 July 1996, discussed in detail above, where the score is close to one for precipitation totals of 2 mm and still 0.5 for the 10 mm threshold.

On the contrary, the cases of July 1994 are exhibiting low scores and this points to the not sufficiently accurate representation of the precipitation processes. These episodes were of more local character (see, e.g., the number of grid cells receiving 1 mm in Fig. 8) and were

induced by rapidly growing mesoscale convective systems. Although DM exhibits some skill in capturing the meso-scale evolution of the flow field (for details see Keil and Volkert, 1999) the model fails in reproducing the correct precipitation pattern. Sensitivity experiments (not displayed) show the substantial influence of the time of model initialisation and particularly the crucial character of the humidity fields on the precipitation totals.

Hence, regarding scores of precipitation totals, DM is better suited for the simulation of precipitation events induced by pronounced larger meso-scale flow structures (July 1996 cases) than for events developing on the smaller meso-scale. The large variations found reflect the complexity of the precipitation generation processes and the difficulty of quantitatively predicting rainfall patterns.

6. Diagnostic Study for a Water Shed

After the examination of the model's ability to predict mesoscale precipitation fields in southern Germany we proceed using the DM as a diagnostic tool to inspect the *atmospheric water budget.* The reasonably good agreement with observations qualifies the precipitation episode in early July 1996 to exemplify the analysis of moisture flux. Before the examination of the atmospheric water budget we first investigate the partition of convective and grid-scale precipitation in some more detail.

The considered domain comprises the catchments of the rivers *Isar* and *Amper* south of their confluence near *Freising* in southern Bavaria. It covers 45 model grid-meshes with an area of about 9000 km^2 in the northern Alpine region (see Fig. 7). In Fig. 9 two striking precipitation events are evident within the 4 day episode from 5 July 1996, 06 UT until 9 July 96, 06 UT. A closer inspection reveals their different nature. The convective precipitation dominates in the evening hours on 5 July and is correlated with strong area averaged upward motion up to 23 cm/s prevailing over about 50% of the subdomain (data are taken from the 680 hPa pressure level in a height of about 3 km). In contrast the second rainfall extremum on 8 July is of grid scale nature. Steady upward motion of less than 10 cm/s over the whole subdomain leads to heavy rainfall. This partitioning results in 91% convective precipitation on 5 July versus only 24% on 8 July (Table 2).

While the precipitation event on 5 July is identified with the passage of the strong convergence line, the second maximum on 8 July is caused by quasi-stationary orographic induced lifting processes as mentioned in the previous section. Thus the model captures the different excitation mechanisms of heavy precipitation during this 4 day episode.

Following an approach for climate studies (Schär et al., 1999), we now inspect the atmospheric water budget which comprises the following terms:

$$Fq_D + Fq_w + EV + \Delta Q - RR = Res$$

where Fq_i represents the netto flux of moisture ($Fq_i = Fq_{i,in} - Fq_{i,out}$; q_D: water vapor; q_w: liquid water), EV evapotranspiration, ΔQ the storage of water in the control volume, RR precipitation, while Res designates a residual which ideally should vanish. The vertically integrated moisture flux is averaged over the already mentioned subdomain of the *Isar-Amper* catchment.

The temporal evolution of the moisture flux shows a rather complex and spiky behaviour during the passage of the convergence line on 5 July (Fig. 10). This can partly be attributed to the discrete nature of the budget calculation from hourly model output fields and partly to the small size of the subdomain comprising only 5×9 grid cells. Nonetheless some insight can be gained from the displayed timeseries of the main terms forming the atmospheric water budget. While the first spell of rain at 14 UT is dominated by the moisture advection Fq_D the second precipitation event at about 20 UT on 5 July mainly originates from the lifting of the humid air (stored in ΔQ) which was advected (Fq_D) earlier that day. As shown in Fig. 9 the strong upward motion period is very well correlated with episodes of heavy precipitation. Unless strong upward motion is present in the small control volume the moisture advection Fq_D is mainly balanced by the storage term ΔQ (e.g., on 7 July). The orographic precipitation on 8 July is nourished by a combination of moisture advection and the release of stored humidity. The advection of

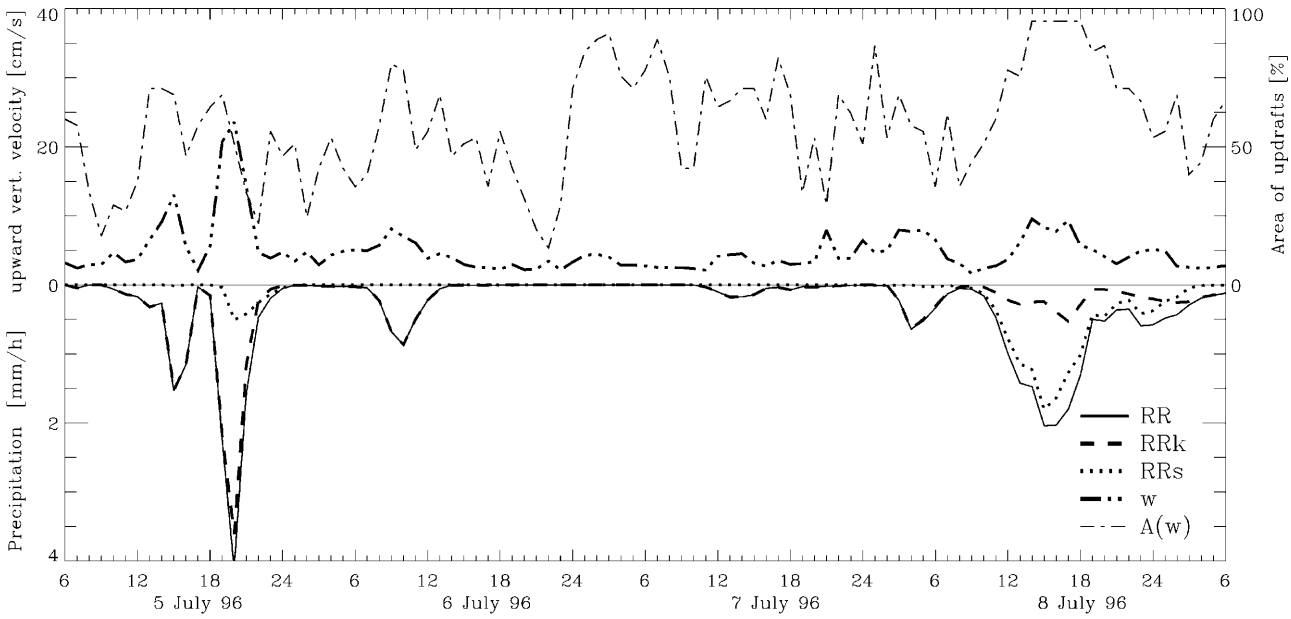

Fig. 9. Timeseries of the convective (*RRk*) and grid scale (*RRs*) components of precipitation and the vertical velocity (w, in 680 hPa or about 3 km; only upward motion) together with its areal exteant [A(w)] in the *Isar-Amper* catchment from 5 July 1996, 06 UT until 9 July 1996, 06 UT

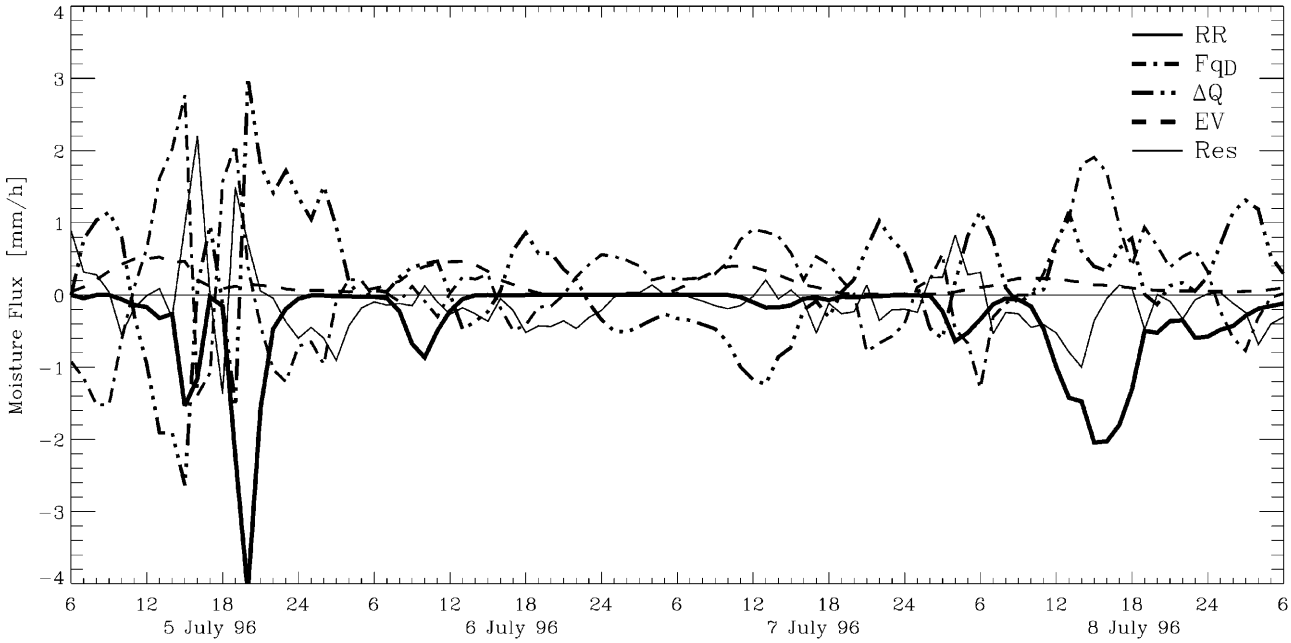

Fig. 10. Timeseries of the moisture fluxes contributing to the atmospheric water budget averaged over the *Isar-Amper* catchment for the same 4 day episode as in Fig. 9; explanation of letter codes in the text

cloud water Fq_W is negligible throughout the whole episode (not displayed). Autochthonous influences, through term *EV,* contribute comparatively little to overall *RR* partly owing to the smallness of the control volume. However the dependence of the evapotranspiration on the solar insolation with its maximum around noon becomes clearly evident. On 8 July evapotranspiration is reduced by a compact cloud system which inhibited insolation.

7. Conclusions

The thorough case-study-type inspection of simulated precipitation signatures gives indications of the model's ability to properly represent the circulation features that actually occurred in nature. Observational data from different sources comprising traditionally used rain gauge measurements, timeseries of meteorological parameters and radar data were complementary used for the assessment of DM's capabilities to simulate different precipitation regimes.

Using these various observations a detailed model validation for the 5 July 1996 case study was performed. An inspection of the 24 hourly precipitation distribution shows minor differences and the error in the mean accumulated rainfall amounts to less than 10%. The horizontal progression of the precipitation fields, as compared with radar reflectivity data, shows the model's ability to catch the fundamental frontal characteristics in the meso-scale. Yet applying Tiedtke's convective mass flux scheme in the meso-scale yields rather patchy instantaneous rain-rate signatures. The identified temporal discrepancy of about one hour is not infrequent in mesoscale modelling and explained by deficiencies in the data at the model boundaries (Haase et al., 1997; Majewski, 1997) and the insufficient model resolution. Particularly the comparison of radar derived wind data and the simulated winds shows the capability to reproduce the observed meso-scale flow field reasonably well. On the other hand the timeseries elucidate the limitation of the hydrostatic model in precisely describing the sudden passage of a well developed convergence line.

Subsequently the bias and the threat scores were applied to obtain compact quantitative measures of the model's quality to capture different precipitation regimes. These exacting scores illustrate the larger skill of the model to simulate precipitation structures of meso-α-scale extent, i.e. higher scores were obtained for the 5 July and 8 July 1996 than for the two Mesoscale Convective Systems in 1994 (Fig. 8).

The inspection of the temporal evolution of the partition of precipitation in combination with the mean upward vertical velocity averaged over the control domain in the northern Alpine foreland revealed the model's skill in capturing the different excitation mechanisms of precipitation during the 4 day episode in early July 96. Diagnosing the components of the atmospheric water budget gave further insight in their different behavior during varying synoptic conditions.

Finally the Deutschland Modell was found to be well suited for the simulation of precipitation events induced by pronounced meso-scale flow structures as was illustrated by the reported case of early July 1996 and the initiation phase of the Oder floods the following year (see Keil et al., 1999). The model's limitations are reached when simulating the MCSs of 1994. Here the DM failed to predict the timing of the precipitation as well as the rainfall amount in the northern Alpine region. Sensitivity studies outline the importance of the initialisation time and its humidity distribution.

In summary, we conclude that the quantitative simulation of precipitation has growing potential to provide valuable information for a follow-on hydrological simulation for sufficiently large river basins and aiming at flood warnings. The validation techniques, which were presented here, should be further applied to monitor the atmospheric simulation quality. An important breakthrough is envisaged when non-hydrostatic simulation models with solely explicit precipitating ice-phase processes on horizontal resolutions of a few kilometres, for which research applications are available (Stein et al., this volume; Benoit et al., 2000), will be transferred to operational use.

Acknowledgements

We thank Detlev Majewski (DWD, Offenbach) for his support with the Deutschland Modell and for providing the DM-analysis data. Daniel Lüthi (ETH, Zürich) kindly made available the code for the budget calculations. Two referees provided valuable comments to strengthen the line of argumentation. This study was in parts supported by the European Commission, Programme "Environment and Climate" under contract ENV4-CT96-0332.

References

Anthes, R. A., 1983: Regional models of the atmosphere in middle latitudes. *Mon. Wea. Rev.,* **111**, 1306–1335.

Bebber, W. J. van, 1891: Die Zugbahnen der barometrischen Minima. *Meteorol. Z.,* **8**, 361–366 (plus xii plates).

Benoit, R., Pellerin, P., Kouwen, N., Ritchie, H., Donaldson, N., Joe, P., Soulis, R., 2000: Toward the use of coupled atmospheric and hydrologic models at regional scale. *Mon. Wea. Rev.,* (accepted).

Frei, C., Schär, C., 1998: A precipitation climatology of the Alps from high-resolution rain-gauge observations. *Int. J. Climatol.,* **18**, 873–900.

Joss, J., Lee, R., 1995: The application of radar-gauge comparisons to operational precipitation profile corrections. *J. Appl. Meteor.,* **34**, 2612–2630.

Haase-Straub, S. P., Hagen, M., Hauf, T., Heimann, D., Peristeri, M., Smith, R. K., 1997: The squall-line of 21 July 1992 in southern Germany: An observational case study. *Beitr. Phys. Atmos.,* **70**, 147–165.

Hagen, M., Schiesser, H.-H., Dorninger, M., 2000: Monitoring of mesoscale precipitation systems in the Alps and the northern Alpine foreland by radar and rain gauges. *Meteorol. Atmos. Phys.,* **72**, 87–100.

Keil, C., Volkert, H., Majewski, D., 1999: The Oder flood in July 1997: Transport routes of precipitable water diagnosed with an operational forecast model. *Geophys. Res. Lett.,* **26**, 235–238.

Keil, C., Volkert, H., 1999: Radar composites and mesoscale precipitation forecasts: Determination of model deficiencies through case studies. Proceed. Final Conf. of COST 75 activity: Advanced weather radar systems, CEC, Luxembourg, ISBN 92-828-4907-4, 407–417.

Majewski, D., 1997: Operational regional prediction. *Meteorol. Atmos. Phys.,* **63**, 89–104.

Molinari, J., Dudek, M., 1992: Parameterization of convective precipitation in mesoscale numerical models: A critical review. *Mon. Wea. Rev.,* **120**, 326–344.

Schär, C., Lüthi, D., Beyerle, U., Heise, E., 1999: The soil-precipitation feedback: A process study with a regional climate model. *J. Climate,* **12**, 722–741.

Schrodin, R. (ed.), 1997: Quarterly Report of the operational NWP-Models of the Deutscher Wetterdienst. Available from DWD, Postfach 100465, D-63004 Offenbach, Germany.

Stein, J., Richard, E., Lafore, J. P., Pinty, J. P., Ascencio, N., Cosma, S., 1999: High-resolution non-hydrostatic simulations of flash-flood episodes with grid-nesting and ice-phase parameterization. *Meteorol. Atmos. Phys.,* **72**, 203–221.

Volkert, H., 2000: Heavy Precipitation in the Alpine Region (HERA): Areal rainfall determination for flood warnings through in-situ measurements, remote sensing and atmospheric modelling. *Meteorol. Atmos. Phys.,* **72**, 73–85.

Tiedtke, M., 1989: A comprehensive mass flux scheme for cumulus parameterization in large-scale models. *Mon. Wea. Rev.,* **117**, 1779–1800.

Authors' address: Christian Keil and Hans Volkert, DLR, Institut für Physik der Atmosphäre, D-82234 Wessling, Germany (e-mail: Christian.Keil@dlr.de, Hans.Volkert@dlr.de).